



CHORUS

This is the accepted manuscript made available via CHORUS. The article has been published as:

Magnetic-field-induced decrease of the spin Peltier effect in $\text{Pt/Y}_{\{3\}}\text{Fe}_{\{5\}}\text{O}_{\{12\}}$ system at room temperature

Ryuichi Itoh, Ryo Iguchi, Shunsuke Daimon, Koichi Oyanagi, Ken-ichi Uchida, and Eiji Saitoh

Phys. Rev. B **96**, 184422 — Published 20 November 2017

DOI: [10.1103/PhysRevB.96.184422](https://doi.org/10.1103/PhysRevB.96.184422)

Magnetic-field-induced decrease of spin Peltier effect in Pt/Y₃Fe₅O₁₂ system at room temperature

Ryuichi Itoh,¹ Ryo Iguchi,^{1,2,*} Shunsuke Daimon,^{1,3} Koichi
Oyanagi,¹ Ken-ichi Uchida,^{2,4,5} and Eiji Saitoh^{1,3,5,6}

¹*Institute for Materials Research, Tohoku University, Sendai 980-8577, Japan*

²*National Institute for Materials Science, Tsukuba 305-0047, Japan*

³*WPI Advanced Institute for Materials Research,
Tohoku University, Sendai 980-8577, Japan*

⁴*PRESTO, Japan Science and Technology Agency, Saitama 332-0012, Japan*

⁵*Center for Spintronics Research Network,
Tohoku University, Sendai 980-8577, Japan*

⁶*Advanced Science Research Center,
Japan Atomic Energy Agency, Tokai 319-1195, Japan*

Abstract

We report the observation of magnetic-field-induced decrease of the spin Peltier effect (SPE) in a junction of a paramagnetic metal Pt and a ferrimagnetic insulator Y₃Fe₅O₁₂ (YIG) at room temperature. For driving the SPE, spin currents are generated via the spin Hall effect from applied charge currents in the Pt layer, and injected into the adjacent thick YIG film. The resultant temperature modulation is detected by a commonly-used thermocouple attached to the Pt/YIG junction. The output of the thermocouple shows sign reversal when the magnetization is reversed and linearly increases with the applied current, demonstrating the detection of the SPE signal. We found that the SPE signal decreases with the magnetic field. The observed decreasing rate was found to be comparable to that of the spin Seebeck effect (SSE), suggesting the dominant and similar contribution of the low-energy magnons in the SPE as in the SSE.

I. INTRODUCTION

Thermoelectric conversion is one of the promising technologies for smart energy utilization¹. Owing to the progress of spintronics in this decade, the spin-based thermoelectric conversion is now added to the scope of the thermoelectric technology²⁻⁷. In particular, the thermoelectric generation mediated by flow of spins, or spin current, has attracted much attention because of the advantageous scalability, simple fabrication processes, and flexible design of the figure of merit^{4,8-12}. This is realized by combining the spin Seebeck effect (SSE)¹³ and spin-to-charge conversion effects¹⁴⁻¹⁶, where a spin current is generated by an applied thermal gradient and is converted into electricity owing to spin-orbit coupling.

The SSE has a reciprocal effect called the spin Peltier effect (SPE), discovered by Flipse *et al.* in 2014 in a Pt/yttrium iron garnet ($\text{Y}_3\text{Fe}_5\text{O}_{12}$: YIG) junction^{5,17}. In the SPE, a spin current across a normal conductor (N)/ferromagnet (F) junction induces a heat current, which can change the temperature distribution around the junction system.

To reveal the mechanism of the SPE, systematic experiments have been conducted¹⁷⁻¹⁹. Since the SPE is driven by magnetic fluctuations (magnons) in the F layer, detailed study on the magnetic-field and temperature dependence is indispensable for clarifying the microscopic relation between the SPE and magnon excitation and the reciprocity between the SPE and SSE²⁰⁻³⁰. A high magnetic field is expected to affect the magnitude of the SPE signal via the modulation of spectral properties of magnons. In fact, the SSE thermopower in a Pt/YIG system was shown to be suppressed by high magnetic fields not only at low temperatures but also at room temperature; the decreasing rate is much greater than the conventional theoretical expectation based on the equal contribution over the magnon spectrum. It highlights the dominant contribution of sub-thermal magnons, which possess lower energy and longer propagation length than thermal magnons^{22-24,29,31-34}. Thus, the experimental examination of the field dependence of the SPE is an important task for understanding the SPE. Although the SPE has recently been measured in various systems by using the lock-in thermography (LIT)¹⁷, it is difficult to be used at high fields and/or low temperatures. For investigating the high-magnetic-field response of the SPE, an alternative method is required.

In this paper, we investigate the magnetic field dependence of the SPE up to 9 T at 300 K by using a commonly-used thermocouple (TC) wire. As revealed by the LIT experiments^{17,19},

the temperature modulation induced by the SPE is localized in the vicinity of N/F interfaces. This is the reason why the magnitude of the SPE signals is very small in the first experiment by Flipse *et al.*⁵, where a thermopile sensor is put on the bare YIG surface, not on the Pt/YIG junction. Here, we show that the SPE can be detected with better sensitivity simply by attaching a common TC wire on a N/F junction. This simple SPE detection method enables systematic measurements of the magnetic field dependence of the SPE, since it is easily integrated to conventional measurement systems. In the following, we describe the details of the electric detection of the SPE signal using a TC, the results of the magnetic field dependence of the SPE signal in a high-magnetic-field range, and its comparison to that of the SSE thermopower.

II. EXPERIMENTAL

The spin current for driving the SPE is generated via the spin Hall effect (SHE) from a charge current applied to N^{15,16}. The SHE-induced spin current then forms spin accumulation at the N/F interface, whose spin vector representation is given by

$$\boldsymbol{\mu}_s \propto \theta_{\text{SHE}} \mathbf{j}_c \times \mathbf{n}, \quad (1)$$

where θ_{SHE} is the spin Hall angle of N, \mathbf{j}_c the charge-current-density vector, and \mathbf{n} the unit vector normal to the interface directing from F to N. $\boldsymbol{\mu}_s$ at the interface exerts spin-transfer torque to magnons in F via the interfacial exchange coupling at finite temperatures, when $\boldsymbol{\mu}_s$ is parallel or anti-parallel to the equilibrium magnetization (\mathbf{m})^{35,36}. The torque increases or decreases the number of the magnons depending on the polarization of the torque ($\boldsymbol{\mu}_s \parallel \mathbf{m}$ or $\boldsymbol{\mu}_s \parallel -\mathbf{m}$), and eventually changes the system temperature by energy transfer, concomitant with the spin-current injection^{5,17,30}. The energy transfer induces observable temperature modulation in isolated systems, which satisfies the following relation

$$\Delta T_{\text{SPE}} \propto \boldsymbol{\mu}_s \cdot \mathbf{m} \propto (\mathbf{j}_c \times \mathbf{n}) \cdot \mathbf{m}. \quad (2)$$

A schematic of the sample system and measurement geometry is shown in Fig. 1(a). The sample system is a Pt strip on a single-crystal YIG. The YIG layer is 112- μm -thick and grown by a liquid phase epitaxy method on a 500- μm -thick $\text{Gd}_3\text{Ga}_5\text{O}_{12}$ substrate with the lateral dimension $10 \times 10 \text{ mm}^2$, where small amount of Bi is substituted for the Y-site of

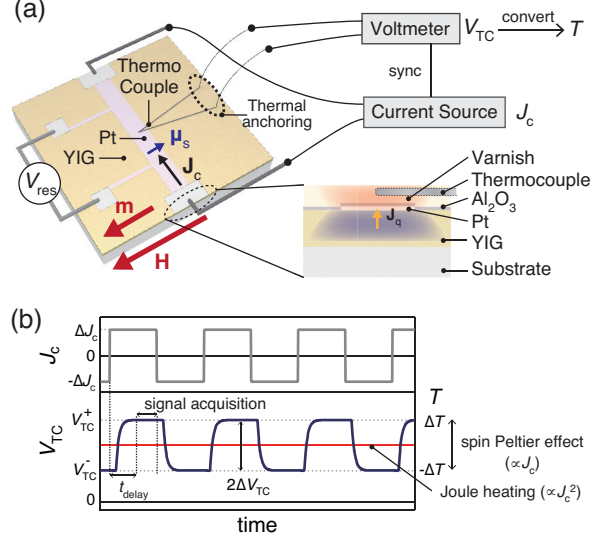


FIG. 1. (a) Schematic of the Pt/YIG sample and measurement system with a thermocouple wire. \mathbf{J}_c , $\boldsymbol{\mu}_s$, \mathbf{m} , \mathbf{H} , and \mathbf{J}_q denote the applied current, the spin accumulation, the unit vector of the equilibrium magnetization, the magnetic field, and the heat current concomitant with the spin-current injection. In an isolated system, \mathbf{J}_q induces a temperature gradient by accumulating heat, which can be detected by the thermocouple. The resistance of the Pt strip is obtained by measuring V_{res} . The measurements were carried out by using the physical property measurement system, Quantum Design. (b) Expected responses due to the SPE and Joule heating when J_c is periodically changed from ΔJ_c to $-\Delta J_c$ with the zero offset current $J_c^0 = 0$. Corresponding voltage signals V_{TC}^+ and V_{TC}^- are obtained after the time delay t_{delay} . The SPE signal is extracted from the difference $\Delta V_{\text{TC}} = (V_{\text{TC}}^+ - V_{\text{TC}}^-) / 2$.

the YIG to compensate the lattice mismatching to the substrate. The Pt strip, connected to four electrodes, is 5-nm-thick, 0.5-mm-wide, fabricated by a sputtering method, and patterned with a metal mask. Then, the whole surface of the sample except the electrodes is covered by a highly-resistive Al_2O_3 film with a thickness of ~ 100 nm by means of an atomic layer deposition method. We attached a TC wire to the top of the Pt/YIG junction, where the wire is electrically insulated from but thermally connected to the Pt layer owing to the Al_2O_3 layer. We used a type-E TC with a diameter of 0.013 mm (Omega engineering CHCO-0005), and fixed its junction part on the middle of the Pt strip using varnish. The rest of the TC wires were fixed on the sample surface for thermal-anchoring and avoiding thermal leakage from the top of the Pt/YIG junction [see the cross sectional view in Fig.

1(a)]. The expected thickness of the varnish between the TC and the sample surface is in the order of $10 \mu\text{m}$ ³⁷. Note that the thickness of the varnish layer does not affect the magnitude of the signal while it affects the temporal response of the TC³⁸. The ends of the Pt strip are connected to a current source and the other two electrodes are used for measuring resistance based on the four-terminal method. The magnetic field \mathbf{H} is applied in the film plane and perpendicular to the strip, thus is along $\boldsymbol{\mu}_s$, satisfying the symmetry of the SPE [Eq. (2)]. The TC is connected to electrodes on a heat bath, which acts as a thermal anchor, and further connected to a voltmeter via conductive wires. The measurements were carried out at 300 K and $\sim 10^{-3}$ Pa.

For the electric detection of the SPE, we measured the amplitude difference (ΔV_{TC}) of the TC voltage V_{TC} in response to a change (ΔJ_c) in the current J_c (so-called Delta-mode of the nanovoltmeter Keithley 2182A). After the current is set to $J_c = J_c^0 \pm \Delta J_c$, time delay (t_{delay}) is inserted before measuring the corresponding voltages V_{TC}^{\pm} . Then, ΔV_{TC} is obtained as $\Delta V_{\text{TC}} = (V_{\text{TC}}^+ - V_{\text{TC}}^-) / 2$. The time delay t_{delay} is necessary because the temperature modulation occurred at the Pt/YIG junction takes certain time to reach and stabilize the TC. The appropriate value of t_{delay} can be determined from the delay-dependence of the SPE signal, which will be shown in Sec. III. For the SPE measurements, we set no offset current ($J_c^0 = 0$) so that ΔV_{TC} is free from Joule heating ($\propto J_c^2$), and the SPE ($\propto J_c$) is expected to dominate the ΔV_{TC} signal [see Fig. 1(a)]. By using the measured values of ΔV_{TC} , the temperature modulation (ΔT) is estimated via the relation $\Delta T = S_{\text{TC}} \Delta V_{\text{TC}}$, where S_{TC} is the Seebeck coefficient of the TC. For the low-field measurements ($\mu_0 H < 0.1$ T), the reference value of $S_{\text{TC}} = 61 \mu\text{V}/\text{K}$ at 300 K is used, while, for the high-field measurements, the field dependence of S_{TC} , determined by the method shown in Appendix A, is used.

III. RESULTS AND DISCUSSION

First, we demonstrated the electric detection of the SPE at low fields. Figure 2(a) shows ΔV_{TC} as a function of the field magnitude H at $\Delta J_c = 10$ mA and $t_{\text{delay}} = 50$ ms. ΔV_{TC} clearly changes its sign when the field direction is reversed and the appearance of the hysteresis demonstrates that it reflects the magnetization curve of the YIG, showing the symmetry expected from Eq. (2)^{5,17}. The small offset of ΔV_{TC} may be attributed to the temperature modulation by the Peltier effect appearing around the current electrodes, Joule heating due

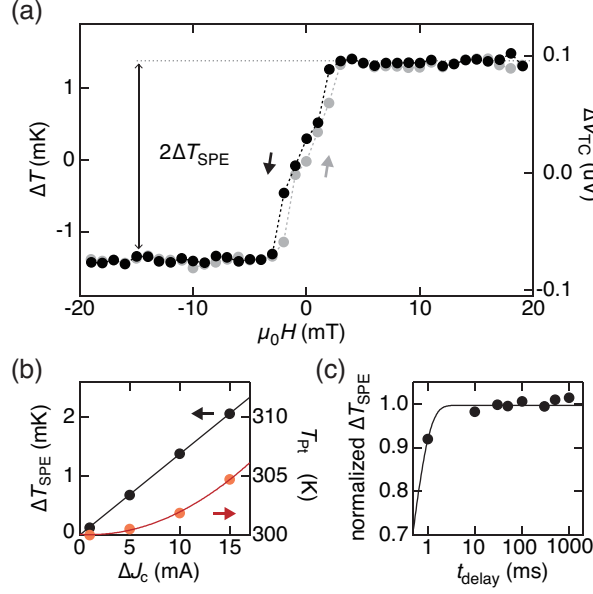


FIG. 2. (a) Field magnitude H dependence of ΔV_{TC} (the right axis) and ΔT without offset (the left axis), measured at $\Delta J_c = 10$ mA and $t_{delay} = 50$ ms. (b) Current J_c dependence of ΔT_{SPE} at $\mu_0 |H| = 0.1$ T, where μ_0 represents the permeability of vacuum. (c) Delay-time t_{delay} dependence of ΔT_{SPE} . Plotted data are estimated from the results measured at $\Delta J_c = 10$ mA and $5 \text{ mT} < \mu_0 |H| < 20 \text{ mT}$ and normalized based on the fitting with $B[1 - \exp(-t_{delay}/\tau)]$, where B denotes the proportional constant and $\tau = 0.4$ ms denotes the characteristic time scale. The acquisition time of 20 ms is used for measurements.

to small uncanceled current offsets, and possible electrical leakage of the applied current from the sample to the TC. Since the Peltier and resistance effects are of even functions of the magnetization cosines though the SPE is of an odd function, the SPE-induced temperature modulation ΔT_{SPE} can be extracted by subtracting the symmetric response to the magnetization: $\Delta T_{SPE} = [\Delta T(+H) - \Delta T(-H)]/2^5$. Figure 2(b) shows the ΔJ_c dependence of ΔT_{SPE} and the temperature (T_{Pt}) of the Pt strip, estimated from the resistance of the strip. While T_{Pt} increases parabolically with the magnitude of ΔJ_c for Joule heating, ΔT_{SPE} increases linearly as is expected from the characteristic of the SPE. This distinct dependencies show negligibly small contribution to ΔT_{SPE} from the Joule heating in this study³⁹. The magnitude of the SPE signal is estimated to be $\Delta T_{SPE}/\Delta j_c = 3.4 \times 10^{-13} \text{ Km}^2/\text{A}$, where Δj_c is the difference in j_c . This value is almost same as the value obtained in the thermographic experiments^{17,19}; since in Ref.¹⁹ the sine-wave amplitude A of ΔT_{SPE} is di-

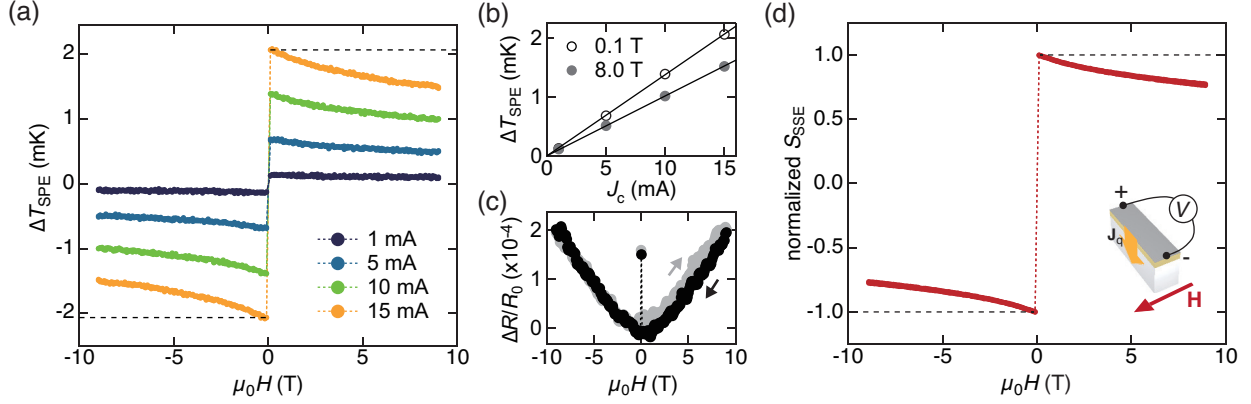


FIG. 3. (a) Field dependence of ΔT_{SPE} including the high-magnetic-field range measured at various ΔJ_c values. (b) J_c dependence of ΔT_{SPE} at $\mu_0 |H| = 0.1$ T and 8.0 T. The solid lines represent the linear fitting. (c) Field dependence of the resistance change $\Delta R = R(H) - R_0$, where R denotes the resistance and R_0 that at $\mu_0 H = 0.1$ T. (d) Field dependence of the spin Seebeck voltage V_{SSE} normalized at $\mu_0 H = 0.1$ T, where V_{SSE} is obtained by measuring the voltage under heater power of 100 mW and subtracting the component symmetric to H .

vided by the rectangular-wave amplitude of Δj_c , a correction factor of $\pi/4$ is necessary, i.e. $\Delta T_{\text{SPE}}/\Delta j_c = \pi A/(4\Delta j_c) = 3.7 \times 10^{-13}$ Km²/A in the previous study. We note that, in the above and following measurements, $t_{\text{delay}} = 50$ ms is chosen based on the t_{delay} dependence of ΔT_{SPE} [Fig. 2(c)], where ΔT_{SPE} is almost saturated at $t_{\text{delay}} > 10$ ms. Such finite but small thermal-stabilization time can be explained by the thermal diffusion from the junction to the TC and rapid thermal stabilization of the SPE-induced temperature modulation¹⁷.

Next, we measured the field dependence of the SPE at higher fields up to $\mu_0 H = 9.0$ T. Figure 3(a) shows ΔT_{SPE} as a function of H , where ΔJ_c is changed from 1 to 15 mA. The decrease of the ΔT_{SPE} signal at higher fields is clearly observed for all the ΔJ_c values. As shown in Fig. 3(b), the signal shows a linear variation with J_c both at $\mu_0 H = 0.1$ T and 8.0 T, demonstrating a constant decreasing rate. Since the resistance of the sample varies only 1 % at most [Fig. 3(c)], the junction temperature keeps constant during the field scan. The field dependence of the thermal conductivity of YIG is also irrelevant to the ΔT_{SPE} suppression as it is known to be negligibly small at room temperature⁴⁰. Thus we can conclude that the decrease is attributed to the nature of the SPE. By calculating the

magnitude of the decrease as

$$\delta_{\text{SPE}} = 1 - \frac{\Delta T_{\text{SPE}}(\mu_0 H = 8.0 \text{ T})}{\Delta T_{\text{SPE}}(\mu_0 H = 0.1 \text{ T})},$$

we obtained $\delta_{\text{SPE}} = 0.26$.

To compare δ_{SPE} to the field-induced decrease of the SSE, we performed SSE measurements in a longitudinal configuration using a Pt/YIG junction system fabricated at the same time as the SPE sample. The SSE sample has the lateral dimension $2.0 \times 6.0 \text{ mm}^2$ and the same vertical configuration as the SPE sample except for the absence of the Al_2O_3 layer. The detailed method of the SSE measurement is available elsewhere^{28,41,42}. Figure 3(d) shows the field dependence of the SSE thermopower in the Pt/YIG junction. The clear decrease of the SSE thermopower is observed. Importantly, the high-field response of the SSE is quite similar to that of the SPE in the Pt/YIG system. The decreased magnitude of the SSE δ_{SSE} , defined in the same manner as the SPE, is estimated to be ~ 0.22 , consistent with the previously reported values^{22–24}.

The observed remarkable field-induced decrease of the SPE at room temperature shows that the SPE is likely dominated by low-energy magnons because the energy scale of the applied field is less than 10 K and thus much lower than the thermal energy of 300 K²². The origin of the strong contribution of the low-energy magnons in the SPE can be (i) stronger coupling of the spin torque to the low-energy (sub-thermal) magnons and (ii) greater propagation length of the low-energy magnons than those of high-energy (thermal) magnons³⁴. While (i) is not well experimentally investigated, the existence of the μm -range length scale in the SPE¹⁹ and the similarity between δ_{SPE} and δ_{SSE} suggest the dominant contribution from (ii) as in the case of the SSE^{24,34}. In fact, recently, it has been demonstrated that the high magnetic fields reduce the propagation length of magnons contributing to the SSE³⁴. This length-scale scenario can qualitatively explain the decrease in the SPE. Recalling that a heat current density (j_q) existing over a distance (l) generates the temperature difference $\Delta T = \kappa^{-1} j_q l$ in an isolated system, ΔT should decrease when l decreases, where κ is the thermal conductivity of the system. In the SPE, l corresponds to the magnon propagation length⁴³, and a flow of magnons accompanies a heat current⁴⁰. Consequently, when the high magnetic field is applied and the magnons with longer propagation length are suppressed by the Zeeman gap, the averaged magnon propagation length decreases and thus results in the reduced ΔT . To further investigate the microscopic mechanism of the SPE, consideration

of the spectral non-uniformity may be vital both in experiments and theories.

IV. SUMMARY

In this study, we showed the magnetic field dependence of the spin Peltier effect (SPE) up to 9.0 T at 300 K in a Pt/YIG junction system. We established a simple but sensitive detection method of the SPE using a commonly-available thermocouple wire. The SPE signals were observed to be suppressed at high magnetic fields, highlighting the stronger contribution of low-energy magnons in the SPE. The similar decreasing rate of the SPE-induced temperature modulation to that of the SSE-induced thermopower suggests that the suppression originates the decrease in the magnon propagation length as in the case of the SSE. We anticipate that the experimental results and the method reported here will be useful for systematic investigation of the SPE.

ACKNOWLEDGMENTS

The authors thank T. Kikkawa for the aid in measuring the SSE and G. E. W. Bauer and Y. Ohnuma for the valuable discussion. This work was supported by PRESTO “Phase Interfaces for Highly Efficient Energy Utilization” (Grant No. JPMJPR12C1) and ERATO “Spin Quantum Rectification Project” (Grant No. JPMJER1402) from JST, Japan, Grant-in-Aid for Scientific Research (A) (Grant No. JP15H02012), and Grant-in-Aid for Scientific Research on Innovative Area “Nano Spin Conversion Science” (Grant No. JP26103005) from JSPS KAKENHI, Japan, NEC Corporation, the Noguchi Institute, and E-IMR, Tohoku University. S.D. was supported by JSPS through a research fellowship for young scientists (Grant No. JP16J02422). K.O. acknowledges support from GP-Spin at Tohoku University.

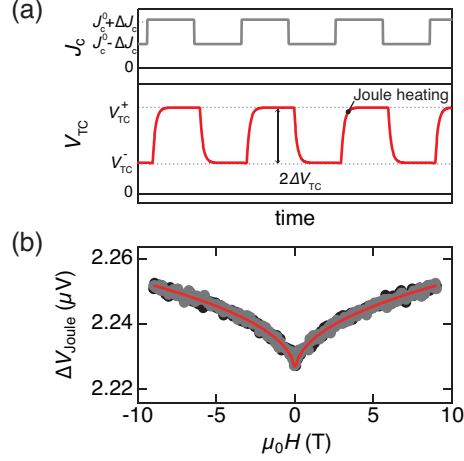


FIG. 4. (a) Expected responses due to the Joule heating at the finite offset current $J_c^0 \neq 0$. (b) Field dependence of ΔV_{Joule} at $\Delta J_c = 0.5$ mA and $J_c^0 = 5$ mA. The solid curve represents the calibration line determined by the fitting.

Appendix A: Calibration of Thermo Couple at High Magnetic Fields

To measure the field dependence of S_{TC} , we used the Joule-heating-induced signal as a reference. By adding a non-zero offset (J_c^0) to the applied current, we obtained the temperature modulation induced by the Joule heating, of which the power P changes from $P(H) = R(H)(J_c^0 - \Delta J_c)^2$ to $P(H) = R(H)(J_c^0 + \Delta J_c)^2$, where R denotes the resistance of the strip [Fig. 4(a)]. Figure 4(b) shows the magnetic field dependence of the component of ΔV_{TC} symmetric to the field ($\Delta V_{\text{Joule}} = [\Delta T_{\text{TC}}(+H) + \Delta T_{\text{TC}}(-H)]/2$). As the change in R , due to the ordinary, spin Hall, and Hanle magnetoresistance effects^{44,45}, is in the order of 0.02 % [Fig.3(c)], its contribution to P can be neglected. Similarly, the field dependence of the thermal conductivity of YIG is negligibly small⁴⁰, ensuring the constant temperature change. Accordingly, the field dependence of ΔV_{Joule} directly reflects $S_{\text{TC}}(H)$. It increases by a factor of ~ 1 % when the field magnitude increases up to 9.0 T. We approximated the field dependence of $S_{\text{TC}}(H)$ as $S_{\text{TC}}(H) = 61(1 + 4.54 \times 10^{-3} |\mu_0 H [\text{T}]|^{0.453})$ [$\mu\text{V}/\text{K}$] by determining the relative change from the measurement results ($\Delta V_{\text{Joule}}(H) / \Delta V_{\text{Joule}}|_{H=0}$) and the absolute value from the reference value.

* IGUCHI.Ryo@nims.go.jp

- ¹ X. Zhang and L.-D. Zhao, *J. Materiomics* **1**, 92 (2015).
- ² G. E. W. Bauer, E. Saitoh, and B. J. van Wees, *Nat. Mater.* **11**, 391 (2012).
- ³ S. R. Boona, R. C. Myers, and J. P. Heremans, *Energy Environ. Sci.* **7**, 885 (2014).
- ⁴ K. Uchida, H. Adachi, T. Kikkawa, A. Kirihara, M. Ishida, S. Yorozu, S. Maekawa, and E. Saitoh, *Proc. IEEE* **104**, 1946 (2016).
- ⁵ J. Flipse, F. K. Dejene, D. Wagenaar, G. E. W. Bauer, J. B. Youssef, and B. J. van Wees, *Phys. Rev. Lett.* **113**, 027601 (2014).
- ⁶ J. Flipse, F. L. Bakker, A. Slachter, F. K. Dejene, and B. J. van Wees, *Nat. Nanotech.* **7**, 166 (2012).
- ⁷ A. Slachter, F. L. Bakker, J. P. Adam, and B. J. van Wees, *Nat. Phys.* **6**, 879 (2010).
- ⁸ K. Uchida, S. Takahashi, K. Harii, J. Ieda, W. Koshibae, K. Ando, S. Maekawa, and E. Saitoh, *Nature* **455**, 778 (2008).
- ⁹ K. Uchida, J. Xiao, H. Adachi, J. Ohe, S. Takahashi, J. Ieda, T. Ota, Y. Kajiwara, H. Umezawa, H. Kawai, G. E. W. Bauer, S. Maekawa, and E. Saitoh, *Nat. Mater.* **9**, 894 (2010).
- ¹⁰ A. Kirihara, K. Uchida, Y. Kajiwara, M. Ishida, Y. Nakamura, T. Manako, E. Saitoh, and S. Yorozu, *Nat. Mater.* **11**, 686 (2012).
- ¹¹ R. Ramos, T. Kikkawa, M. H. Aguirre, I. Lucas, A. Anadón, T. Oyake, K. Uchida, H. Adachi, J. Shiomi, P. A. Algarabel, L. Morellón, S. Maekawa, E. Saitoh, and M. R. Ibarra, *Phys. Rev. B* **92**, 220407 (2015).
- ¹² H. Adachi, K. Uchida, E. Saitoh, and S. Maekawa, *Rep. Prog. Phys.* **76**, 036501 (2013).
- ¹³ K. Uchida, H. Adachi, T. Ota, H. Nakayama, S. Maekawa, and E. Saitoh, *Appl. Phys. Lett.* **97**, 172505 (2010).
- ¹⁴ E. Saitoh, M. Ueda, H. Miyajima, and G. Tatara, *Appl. Phys. Lett.* **88**, 2509 (2006).
- ¹⁵ J. Sinova, S. O. Valenzuela, J. Wunderlich, C. H. Back, and T. Jungwirth, *Rev. Mod. Phys.* **87**, 1213 (2015).
- ¹⁶ A. Hoffmann, *IEEE Trans. Magn.* **49**, 5172 (2013).
- ¹⁷ S. Daimon, R. Iguchi, T. Hioki, E. Saitoh, and K. Uchida, *Nat. Commun.* **7**, 13754 (2016).
- ¹⁸ K. Uchida, R. Iguchi, S. Daimon, R. Ramos, A. Anadón, I. Lucas, P. A. Algarabel, L. Morellón, M. H. Aguirre, M. R. Ibarra, and E. Saitoh, *Phys. Rev. B* **95**, 184437 (2017).
- ¹⁹ S. Daimon, K. Uchida, R. Iguchi, T. Hioki, and E. Saitoh, *Phys. Rev. B* **96**, 024424 (2017).
- ²⁰ K. Uchida, T. Kikkawa, A. Miura, J. Shiomi, and E. Saitoh, *Phys. Rev. X* **4**, 041023 (2014).

- ²¹ S. M. Rezende, R. L. Rodriguez-Suarez, R. O. Cunha, A. R. Rodrigues, F. L. A. Machado, G. A. F. Guerra, J. C. L. Ortiz, and A. Azevedo, *Phys. Rev. B* **89**, 014416 (2014).
- ²² T. Kikkawa, K. Uchida, S. Daimon, Z. Qiu, Y. Shiomi, and E. Saitoh, *Phys. Rev. B* **92**, 064413 (2015).
- ²³ H. Jin, S. R. Boona, Z. Yang, R. C. Myers, and J. P. Heremans, *Phys. Rev. B* **92**, 054436 (2015).
- ²⁴ E. J. Guo, J. Cramer, A. Kehlberger, C. A. Ferguson, D. A. MacLaren, G. Jakob, and M. Kläui, *Phys. Rev. X* **6**, 031012 (2016).
- ²⁵ J. Barker and G. E. W. Bauer, *Phys. Rev. Lett.* **117**, 217201 (2016).
- ²⁶ V. Basso, E. Ferraro, A. Magni, A. Sola, M. Kuepferling, and M. Pasquale, *Phys. Rev. B* **93**, 184421 (2016).
- ²⁷ V. Basso, E. Ferraro, and M. Piazza, *Phys. Rev. B* **94**, 144422 (2016).
- ²⁸ R. Iguchi, K. Uchida, S. Daimon, and E. Saitoh, *Phys. Rev. B* **95**, 174401 (2017).
- ²⁹ A. Miura, T. Kikkawa, R. Iguchi, K. Uchida, E. Saitoh, and J. Shiomi, *Phys. Rev. Materials* **1**, 014601 (2017).
- ³⁰ Y. Ohnuma, M. Matsuo, and S. Maekawa, *Phys. Rev. B* **96**, 134412 (2017).
- ³¹ U. Ritzmann, D. Hinzke, A. Kehlberger, E. J. Guo, M. Kläui, and U. Nowak, *Phys. Rev. B* **92**, 174411 (2015).
- ³² T. Kikkawa, K. Uchida, S. Daimon, and E. Saitoh, *J. Phys. Soc. Jpn.* **85**, 065003 (2016).
- ³³ I. Diniz and A. T. Costa, *New J. Phys.* **18**, 052002 (2016).
- ³⁴ T. Hioki, R. Iguchi, Z. Qiu, D. Hou, K. Uchida, and E. Saitoh, *Appl. Phys. Express* **10**, 073002 (2017).
- ³⁵ Y. Tserkovnyak, A. Brataas, G. E. W. Bauer, and B. I. Halperin, *Rev. Mod. Phys.* **77**, 1375 (2005).
- ³⁶ S. S. L. Zhang and S. Zhang, *Phys. Rev. B* **86**, 214424 (2012).
- ³⁷ This is estimated from the thickness of the varnish layer sandwiched between glass substrates pressed with the same pressure applied to the sample; we pressed the sample and the TC wire with an additional glass cover.
- ³⁸ As the radiation to the outer environment at the surface is negligibly small, the vertical heat current in the varnish layer is zero at the steady-state condition. The effect of the lateral heat currents, expected at the edges of the Pt strip, is also small as the total thickness from the top

of the Pt strip to the surface ($\sim 30 \mu\text{m}$) is smaller than the width ($500 \mu\text{m}$).

- ³⁹ The SPE signal at 305 and 310 K (nominal) was observed to show the same magnitude as that at 300 K. Thus the temperature increase due to the Joule heating does not affect the measured SPE value.
- ⁴⁰ S. R. Boona and J. P. Heremans, *Phys. Rev. B* **90**, 064421 (2014).
- ⁴¹ K. Uchida, T. Ota, H. Adachi, J. Xiao, T. Nonaka, Y. Kajiwara, G. E. W. Bauer, S. Maekawa, and E. Saitoh, *J. Appl. Phys.* **111**, 103903 (2012).
- ⁴² A. Sola, P. Bougiatioti, M. Kuepferling, D. Meier, G. Reiss, M. Pasquale, T. Kuschel, and V. Basso, *Sci. Rep.* **7**, 46752 (2017).
- ⁴³ L. J. Cornelissen, K. J. H. Peters, G. E. W. Bauer, R. A. Duine, and B. J. van Wees, *Phys. Rev. B* **94**, 014412 (2016).
- ⁴⁴ H. Nakayama, M. Althammer, Y. T. Chen, K. Uchida, Y. Kajiwara, D. Kikuchi, T. Ohtani, S. Geprägs, M. Opel, S. Takahashi, R. Gross, G. E. W. Bauer, S. T. B. Goennenwein, and E. Saitoh, *Phys. Rev. Lett.* **110**, 206601 (2013).
- ⁴⁵ S. Vélez, V. N. Golovach, A. Bedoya-Pinto, M. Isasa, E. Sagasta, M. Abadia, C. Rogero, L. E. Hueso, F. S. Bergeret, and F. Casanova, *Phys. Rev. Lett.* **116**, 016603 (2016).